Available online at www.sciencedirect.com
ScienceDirect
ELSEVIER
Palaeogeography, Palaeoclimatology, Palaeoecology 239 (2006) 396–405
PALAEO
www.elsevier.com/locate/palaeo

# Close-up of the end-Permian mass extinction horizon recorded in the Meishan section, South China: Sedimentary, elemental, and biotic characterization and a negative shift of sulfate sulfur isotope ratio

Kunio Kaiho [a,*], Zhong-Qiang Chen [b], Hodaka Kawahata [c], Yoshimichi Kajiwara [d], Hisao Sato [c]

[a] *Institute of Geology and Paleontology, Tohoku University, Sendai 980-8578, Japan*
[b] *School of Earth and Geographical Sciences, The University of Western Australia, Crawley, WA 3009, Australia*
[c] *Geological Survey of Japan, National Institute of AIST, Ibaraki 305-8567, Japan*
[d] *Institute of Geoscience, University of Tsukuba, Ibaraki 305-8571, Japan*

Received 4 July 2005; received in revised form 10 February 2006; accepted 16 February 2006

**Abstract**

The Permian/Triassic (P/Tr) boundary beds of the Meishan section, South China, have been re-studied in detail based on complete samples across the P/Tr transition. Under the microscope, the end-Permian mass extinction horizon is calibrated to a 12-mm stratal interval, the top being 19 mm below the top of Bed 24e of the Changhsing Formation. This abrupt disappearance of skeletal fragments of major benthos characterizes the end-Permian extinction event, suggesting a catastrophic event. An abrupt decrease in the $^{34}S/^{32}S$ ratios of seawater sulfate is confirmed to coincide with the end-Permian event horizon. The sulfur isotope event is thought to have been caused by an overturn of a stratified ocean dominated by $H_2S$, implying coincidence of the oceanic mixing and the mass extinction. Coincident Siberian flood volcanism may have triggered a long-term ($>10^3$ years) cooling leading an ocean mixing. A presumed comet impact to the ocean could have directly caused ocean mixing and the mass extinction.


*Keywords:* mass extinction; permian; triassic; element; fossil; S-34/S-32

## 1. Introduction

The mass extinction event at the end of the Permian killed off over 90% of marine species and ~70% of terrestrial vertebrate families (Erwin, 1994). However, the cause of this severest crisis of Phanerozoic life has long been a subject of conjecture, although multiple interpretations and related evidence have been recently released (e.g., Wignall and Twitchett, 1996; Knoll et al., 1996; Bowring et al., 1998; Kaiho et al., 2001; Wignall, 2001; Becker et al., 2001, 2004; Kidder and Worsley, 2004; Mundil et al., 2004; Grice et al., 2005; Grard et al., 2005; Huey and Ward, 2005). More recently, Xie et al. (2005) assumed that the end-Permian extinction may be multi-episodic rather than mono-episodic based microbial data recorded in the Meishan section. However, an increasing number of studies reveal that an abrupt end-Permian extinction occurred among organisms in both marine and terrestrial environments (Erwin, 1993;

* Corresponding author.
*E-mail address:* kaiho@dges.tohoku.ac.jp (K. Kaiho).

0031-0182/$ - see front matter © 2006 Elsevier B.V. All rights reserved.
doi:10.1016/j.palaeo.2006.02.011

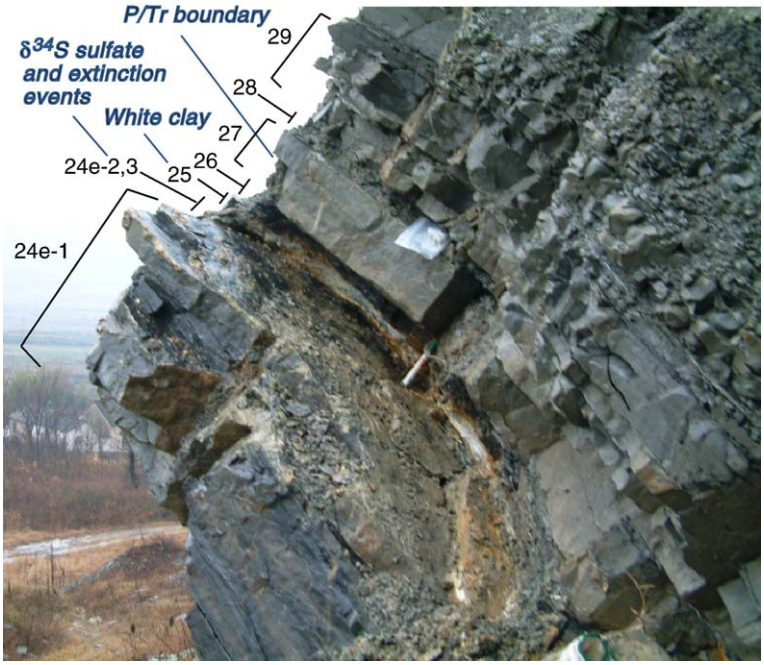


Fig. 1. A photograph of an outcrop of the Meishan A section, South China, showing bed numbers and events.

Retallack, 1995; Eshet et al., 1995; Bowring et al., 1998; Rampino and Adler, 1998; Jin et al., 2000), and Jin et al. (2000) calibrated this event to the base of Bed 25, a white clay bed, at the Meishan section, South China. Although this event has been recognized from many Permian/Triassic (P/Tr) boundary sections around the world, many of the important hypotheses have been proposed based on experimental data sampled from the Meishan section (e.g., Bowring et al., 1998; Jin et al., 2000; Kaiho et al., 2001; Mundil et al., 2001, 2004; Grice et al., 2005; Xie et al., 2005). At Meishan, the P/Tr boundary beds (including Beds 24–28), an approximately 100-cm-thick succession, are crucial in revealing the end-Permian extinction event and the possible causes. Therefore, we herein document the detailed sedimentary, biotic and elemental characterization and of geochemical anomalies (mainly sulfate sulfur isotope ratios) on the basis of relatively complete samples across the P/Tr boundary beds of Meishan. In particular, a pronounced negative shift of $\delta^{34}S_{sulfate}$ values near the end-Permian extinction horizon has been recognized worldwide and attracted more and more attention from many geologists. Kaiho et al. (2001) demonstrated a remarkable decrease in $\delta^{34}S_{sulfate}$ in the ocean at the end of the Permian based on analysis of samples from the P/Tr boundary beds of Meishan. They interpreted this phenomenon as a result of an extraterrestrial impact. This hypothesis was disputed by Koeberl et al. (2002), who noted that Kaiho et al.'s (2001) data do not support the view of an impact event. Ivanov and Melosh (2003) also showed that the Siberian flood basalt volcanism, one of the possible causes triggering the end-Permian extinction (Kamo et al., 2003), could not have been initiated by an extraterrestrial impact. Later, Maruoka et al. (2003) supported the 'sulfur injection' hypothesis based on their finding of high concentrations of sulfide at and just below the terrestrial P/Tr boundary in the northern Karoo Basin, South Africa, and they favored a volcanic sulfur source. More recently, Newton et al. (2004) reported a decrease from ~+20‰ to ~+15‰ in $\delta^{34}S_{sulfate}$ coinciding with the end-Permian mass extinction at Siusi, Italy, although these are based on sporadic samples and there is only one plot showing a low value, ~+15‰. They interpreted the decrease as the result of a global event caused by oceanic mixing. Alternatively, $\delta^{34}S_{sulfate}$ values across the P/Tr boundary in Abadeh, Iran (Korte et al., 2004) do not show a negative shift near the P/Tr boundary. This is most likely because of their sporadic data. We studied fossils under the microscope and found that a pronounced negative shift in sulfate sulfur isotope ratios coincides with the end-Permian extinction horizon, both recorded in a 1-cm-thick limestone layer (see below). This detailed look at palaeontological, sedimentary and geochemical data, based on complete samples from the possible event horizons, may provide insight into the cause of this severe event.

## 2. Stratigraphy and chronology

At Meishan, the P/Tr boundary beds include strata between the topmost Changhsing and lowest Yinkeng Formations. The topmost Changhsing Formation is a limestone bed (Bed 24), which comprises mainly bioclastic packstone (Fig. 1). This bed is of latest Changhsingian (latest Permian) age, falling within the *Clarkina yini* conodont zone (Yin et al., 2001). Overlying Beds 25 and 26 are white claystone (4 cm thick) and black mudstone (6 cm thick), respectively. Bed 27 is composed of a 14-cm-thick marlstone and hosts the P/Tr boundary at its middle portion (Yin et al., 2001). This bed is overlain by a greenish gray clay bed (Bed 28). Jin et al. (2000) calibrated the end-Permian mass extinction horizon to the base of Bed 25 based on the last occurrence of major benthos from the Meishan section. Thus, the topmost Bed 24 (Bed 24e) and Bed 25 are positioned at the end-Permian event horizon below and above, respectively.

Zircon and sanidine dating of the P/Tr boundary of Meishan has been conducted by various laboratories around the world since the early 1990s (e.g., Claoue-Long et al., 1991; Renne et al., 1995). More recently, radiometric ages dated by both Bowring et al. (1998) and Mundil et al. (2001, 2004) are noticeable and widely accepted. When Bowring et al.'s (1998) radiometric ages are followed, depositional ages of Beds 21 (~4.7 m below the P/Tr boundary), 25, 28, and 33 (1.5 m above the P/Tr boundary) are 252.3±0.3 Ma, 251.4±0.3 Ma, 250.7±0.3 Ma, and 250.4±0.5 Ma, respectively. Mundil et al. (2004) provided radiometric ages of 252.4±0.3 Ma for Bed 25 and Mundil et al. (2001) showed an age of 252.5±0.3 Ma for Bed 28.

## 3. Methodology

### 3.1. Sampling

Samples were sawed from the P/Tr beds in the outcrop sections in Meishan. Rock samples from each outcrop section make up one complete lithologic log of the P/Tr transition to ensure no omission of any sedimentary

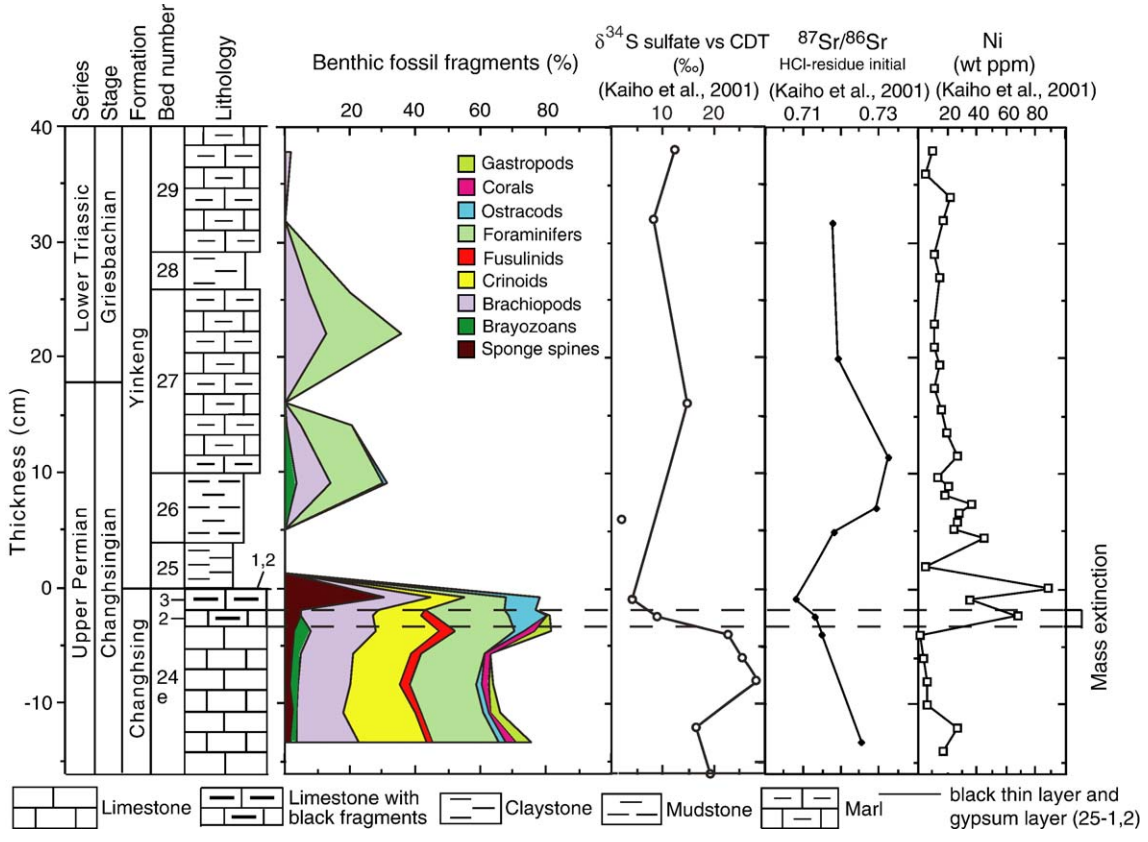


Fig. 2. Variations in lithology, fossils, sulfate sulfur isotope ratio, Sr isotope ratio, and Ni content (bulk) recorded in Upper Permian and Lower Triassic layers at the Meishan A section, South China. Additional fossil fragments analyzed in thin section consist of micrite and silica. Bed numbers are after Yin et al. (1996) and Kaiho et al. (2001). Sulfate sulfur isotope data are after Kaiho et al. (2001).

records across the event horizon. Additional samples, particularly limestone and claystone from Bed 24e and Bed 25, respectively, were also collected to ensure adequate material was available for geochemical analyses. In the laboratory, we conducted fossil and elemental analyses in 0.1-mm to 1-cm-thick stratigraphic slices on well-preserved samples. Numerous thin sections were made from the same horizon to ensure that adequate biotic information could be observed.

### 3.2. Fossil analyses

Theoretically, if an extinction event resulted in the elimination of marine benthos, skeleton fragments recorded in sedimentary rocks should also undergo an abrupt drop in diversity and abundance during the event. Thus, the possible mass extinction horizon can also be determined by changes of skeletal components of various fossil groups in thin sections. Here, a point-counting method is utilized to quantify the occurrence of skeletal fragments of major fossil groups in different horizons under the microscope. The quantitative point count data (Figs. 2, 3) are based on detailed thin sections focusing on microfacies and paleontology of the P/Tr boundary beds. The point-counting data from each thin section are based on observation of 300–350 views in one sample. Then, percentages of various skeletal components, micrite, silica and cavities from samples throughout the section were combined to yield mean abundance of each composition throughout the study succession (Table 1). In addition, the point-counting analyses of 1-mm intervals were conducted between 4.6 cm below and 2 cm above the black thin layer (Bed 25-1).

### 3.3. Elemental abundances in bulk samples

Samples were crushed to fine powder. After drying at 40–50 °C, each sample was split into several sub-samples

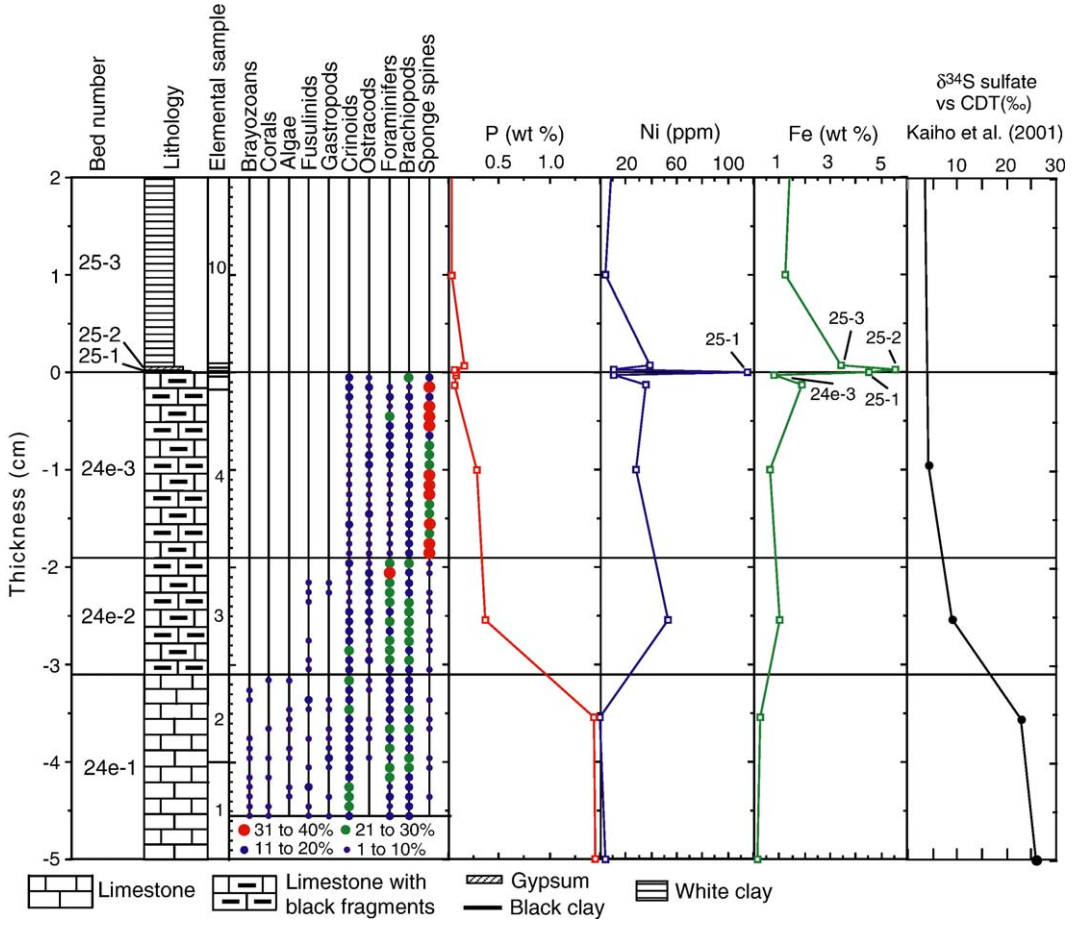


Fig. 3. Variation in lithology, fossils, elements in bulk samples and sulfate sulfur isotope ratio (bulk) across the extinction boundary at the Meishan A section, South China. The reproducibility of these elemental measurements was better than 2%. Sulfate sulfur isotope data are after Kaiho et al. (2001).

Table 1
Geochemical data recorded in Upper Permian and Lower Triassic layers at the Meishan sections

| Sample | Thickness (cm) | $^{87}Sr/^{86}Sr$ HCl-residue initial | $\delta^{34}$Sulfate vs. CDT (‰) | Ca (wt.%) | Ni (wt. ppm) | P (wt.%) | Fe (wt.%) |
|---|---|---|---|---|---|---|---|
| CHMI+37–+39 | 38.000 | | 12.61 | 14.65 | 9.54 | 0.91 | |
| CHMI+35–+37 | 36.000 | | | 15.47 | 5.41 | 0.91 | |
| CHMI+33–+35 | 34.000 | | | 19.58 | 22.22 | 0.90 | |
| CHMI+31–+33 | 32.000 | | 8.17 | 22.98 | 16.74 | 0.90 | |
| CHMIA+30–+33.5 | 31.750 | 0.718 | | | | | 1.74 |
| CHMI+28–+31 | 29.000 | | | 24.43 | 10.70 | 0.86 | |
| CHMI+26–+28 | 27.000 | | | 21.88 | 14.67 | 0.91 | 2.38 |
| CHMI+22–+24 | 23.000 | | | 22.55 | 10.51 | 0.90 | 1.96 |
| CHMI+20–+22 | 21.000 | | | 21.20 | 11.15 | 0.93 | |
| CHMIA+19–+21 | 20.000 | 0.719 | | | | | 1.22 |
| CHMI+19–+20 | 19.500 | | | 20.66 | 14.15 | 0.38 | |
| CHMI+17–+18 | 17.500 | | | 18.79 | 10.96 | 0.25 | |
| CHMIA+15–+17 | 16.000 | | 14.80 | | | | 1.69 |
| CHMI+15–+16 | 15.500 | | | 21.77 | 15.50 | 0.36 | |
| CHMI+13–+14 | 13.500 | | | 21.54 | 19.18 | 0.26 | |
| CHMI+11–+12 | 11.500 | | | 22.72 | 26.91 | 0.27 | |
| CHMIA+10–+13 | 11.500 | 0.733 | | | | | 1.78 |
| CHMI+9.25–+10 | 9.620 | | | 3.15 | 13.77 | 0.27 | |
| CHMI+8.5–+9.25 | 8.880 | | | 0.34 | 20.98 | 0.26 | |
| CHMI+7.75–+8.5 | 8.120 | | | 2.20 | 18.06 | 0.29 | |
| CHMI+7–+7.75 | 7.380 | | | 0.35 | 36.56 | 0.23 | |
| CHMI+6.25–+7 | 6.620 | | | 0.33 | 27.74 | 0.27 | |
| CHMI+5,5–+6.25 | 5.880 | | | 0.48 | 26.14 | 0.28 | |
| CHMI+4.75–+5,5 | 5.120 | | | 0.20 | 24.18 | 0.28 | |
| CHMI+4–+4.75 | 4.380 | | | 0.38 | 44.81 | 0.29 | |
| CHMI+0.3–+4 | 1.900 | | | 0.31 | 4.61 | 0.23 | |
| CHMI+0–+0.3 | 0.150 | | | 0.35 | 87.98 | 0.44 | |
| CHMIA+8–+10 | 9.000 | | | | | | 3.97 |
| CHMIA+6–+8 | 7.000 | 0.729 | | | | | 4.26 |
| CHMIA+4–+10 | 7.000 | | 1.98 | | | | |
| CHMIA+4–+6 | 5.000 | 0.718 | | | | | |
| CHMIA+4–+5 | 4.500 | | | | | | 2.00 |
| CHMI0–+4 | 2.000 | | | 1.67 | 4.42 | 0.03 | |
| CHMIA+0.3–+2 | 1.150 | | | 4.30 | 39.16 | 0.15 | 3.42 |
| CHMIA+0.01–+0.04 | 0.025 | | | 15.15 | 10.73 | 0.05 | 5.53 |
| CHMIA0–+0.01 | 0.005 | | | 1.30 | 115.20 | 0.06 | 4.46 |
| CHMIA−0.05–0 | −0.025 | | | 27.80 | 10.92 | 0.07 | 0.80 |
| CHMIA−0.2–−0.05 | −0.125 | | | 19.57 | 36.28 | 0.05 | 1.92 |
| CHMIA−1–0 | −0.500 | 0.708 | 3.95 | 12.75 | 35.33 | 0.27 | 0.64 |
| CHMIA−2–−1 | −1.500 | 0.713 | 8.99 | 10.40 | 66.97 | 0.36 | 1.02 |
| CHMIA−3–−2 | −2.500 | 0.715 | | | | | |
| CHMI−4–−2 | −3.000 | | 22.91 | 36.53 | 1.65 | 1.43 | 0.27 |
| CHMI−6–−4 | −5.000 | | 25.86 | 36.58 | 4.13 | 1.44 | 0.18 |
| CHMI−8–−6 | −7.000 | | 28.57 | 35.39 | 6.43 | 1.43 | 0.12 |
| CHMI−10–−8 | −9.000 | | | 34.87 | 5.44 | 1.46 | 0.16 |
| CHMI−12–−10 | −11.000 | | 16.63 | 27.81 | 26.79 | 1.33 | 0.56 |
| CHMIA−14–−11 | −12.500 | 0.725 | | | | | |
| CHMI−14–−12 | −13.000 | | | 30.56 | 16.95 | 1.41 | 0.37 |
| CHMI−16–−14 | −15.000 | | 19.60 | | | | |
| CHMI−16 | −16.000 | | | 35.39 | 6.41 | 1.56 | 0.14 |
| CHMI−20–−18 | −19.000 | | 19.85 | | | | |
| CHMI−19–−20 | −19.500 | | | 22.72 | 20.37 | 1.20 | 0.60 |

CHMI: D section, CHMIA: A section. Sample number shows thickness in centimeters in which the base of the Fe-rich black layer is defined as 0 cm; positive and negative numbers correspond to thickness above and below the latter horizon.

for elemental analyses. 100 mg of powdered sample was decomposed by using 5 mL of ultrapure hydrofluoric acid (HF), 3 mL of ultrapure nitric acid ($HNO_3$), and ultrapure hydrochloric acid (HCl) twice. The solution was diluted with 5 mL of concentrated ultrapure nitric acid ($HNO_3$) and double-distilled MILLI-Q water to adjust the total volume to exactly 100 mL. The prepared solution was analyzed by a Seiko SII SPS7800 inductively coupled plasma–atomic emission spectroscopy (ICP-AES) at the Geological Survey of Japan. Estimated by replicate analyses, the precision is within 3%. Reference rock standards provided by the Geological Survey of Japan (JB-1, JB-2, JA-1, JG-1, JG-2 and JR-1) (http://www.aist.go.jp/RIODB/geostand/welcome.html) as well as standard solutions prepared from pure elemental standard solutions were used for calibration. The reproducibility of these measurements was better than 2%.

### 3.4. Sulfur isotope ratio

A bulk powdered sample of the gypsum layer (25-2) was washed by a NaCl solution and then converted to $Ag_2S$ by means of the Kiba-reagent (Sn(II) strong phosphoric acid) method (Sasaki et al., 1979). The $Ag_2S$ precipitates thus obtained are finally converted to $SO_2$ for mass spectrometry by utilizing conventional combustion-distillation techniques in vacuo (Robinson and Kusakabe, 1975). A ratio of masses 66/64 was measured by utilizing a Finnigan Mat delta-E instrument at the Institute of Geosciences, University of Tsukuba. The results of $^{34}S/^{32}S$ ratios are expressed in the conventional permil scale (δ-notation) with respect to the international meteoritic standard CDT (Canyon Diablo Troilite). The overall analytical reproducibility as derived from triplicate analyses of each sample in this study is estimated to be better than ±0.2‰.

### 3.5. Oxygen isotope ratio

A rock sample from Bed 24e-3 is treated with phosphoric acid to isolate silica bars. The $CO_2$-laser microprobe at the Geological Survey of Japan is utilized to measure oxygen isotope ratio of a silica bar from Bed 24e-3.

## 4. Results and discussion

### 4.1. Lithology and sedimentary characterization

As stated above, at Meishan, the top of Changhsing Formation comprises thin-bedded bioclastic packstone (Bed 24). The topmost 40-cm-thick limestone labeled Bed 24e is studied in detail because it is overlain by a white clay bed (Bed 25) and Jin et al. (2000) placed the end-Permian event horizon between these two beds. Bed 24e, except for the topmost 3 cm (24e-2, 24e-3), is dark-gray bioclastic packstone containing abundant calcareous microfossils. The topmost 3 cm (24e-2 and 24e-3) is characterized by low carbonate and high Ni contents (Kaiho et al., 2001; Fig. 2). The basal part of Bed 25 is an Fe- and Ni-rich grayish black thin layer (25-1; black mudstone, 0.1 mm thick; Fig. 3; Table 1). Grayish black, thin fragments are very common in this layer (25-1, 0.1 mm) and the underlying Layers 24e-2 (1 cm thick) and 24e-3 (1 cm). These layers (24e-3 to 25-1) contain Fe–Ni grains (2–50 μm; Kaiho et al., 2001). The overlying thin layer (25-2) is dark yellowish orange, 0.3–1 mm thick and comprises gypsum and Fe (discussed in the Section 4.5). The remaining part of Bed 25 (25-3; 2–4 cm thick) is a bluish gray illite-montmorillonite clay (white clay), which is volcanic ash. The subsequent dark-gray mudstone (Bed 26; 6–8 cm thick) is overlain by a marl bed (Bed 27).

### 4.2. Time scale

Based on radiometric ages dated by Bowring et al. (1998), the duration of the sedimentation of the limestone Bed 24e (40 cm thickness), the dark-gray clay bed (Bed 26) and marl bed (Bed 27) can be estimated approximately as 80 ky, 200 ky, and 500 ky, respectively, except for the layers containing Fe–Ni grains (24e-3, 25-1), gypsum layer (25-2) and volcanic ash (25-3), which are assumed to be essentially instantaneous (<1 ky; Fig. 2).

### 4.3. Possible mass extinction horizon under microscope

Based on quantitative analyses under microscope, fossil components of crinoids, fusulinids, corals, brayozoans, ostracods and gastropods abruptly disappeared within the top 3 cm of Bed 24e (Figs. 2, 3). Palaeozoic corals (attached fauna) have their last occurrence at the top of Bed 24e-1, 32 mm below the top of the Bed 24e. Bryozoans (attached faunas) also disappeared at this horizon (top of Bed 24e-1), but reappeared in Bed 26. The last Permian fusulinids and gastropods (both active epifaunas) occurred at Bed 24e-2, 22 mm below the top of the Bed 24e. Foraminifers and ostracods (both active infaunas) and brachiopods (epifaunas) vanished at the stratal interval 1 mm to 0 mm below the top of Bed 24e and re-occurred in Bed 26. Crinoids (elected attached faunas) also disappeared at the top of Bed 24e. The top 19-mm-thick limestone (Bed 24e-3) is also dominated by

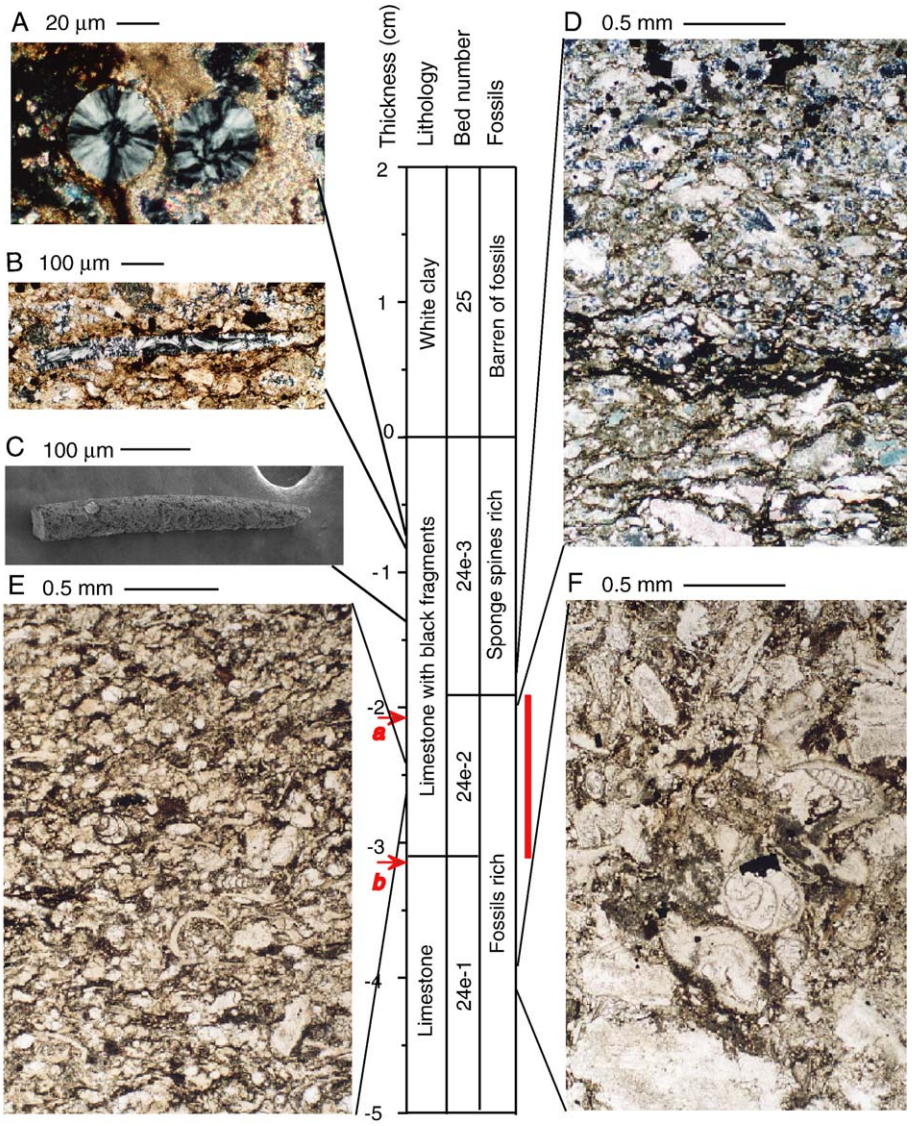


Fig. 4. Fossils at the end-Permian extinction horizon at the Meishan A section, South China. Photographs A and B show sponge spines (silica bars) in thin section in Bed 24-3 ((A) cross sections of spines; (B) a longitudinal section of a spine). Photograph (C) by SEM illustrates a sponge spine extracted from Bed 24-3. Photographs (D–F) show transmitted light microscopic observation of thin sections. (D) was taken using cross Nicol; and (E and F) using open Nicol. Blue grains in (D) are sponge spines. The scale of thickness of the sediments is the same as that in Fig. 3. Red arrows (a) Last occurrence of fusulinids. (b) Last occurrence of Paleozoic coral fragments. The red bar on the column shows the level of mass extinction and a negative shift of sulfate sulfur isotope ratio. (For interpretation of the references to colour in this figure legend, the reader is referred to the web version of this article.)

silica bars, some of which are circular in section and, thus, superficially resemble microspherules or tektites of an impact origin (Fig. 4). However, the $\delta^{18}O_{SMOW}$ value of +23.35‰ measured from the silica bars indicates that these silica bars were precipitated from seawater and, therefore, are not microspherules or tektites. Alternatively, these silica bars are very similar to the silicified skeletons of organisms. Their morphology suggests that these silica bars are actually sponge spines. The elongate bars we observed are longitudinal outlines and the circular grains are cross sections of spines (Fig. 4). This identification is also reinforced by abundant isolated silicified sponge spine specimens extracted from Bed 24e-3 (Fig. 4). These sponge spines were also observed by Jin et al. (Jin, oral presentation in Chaohu, 2005).

The major disappearance boundary of Palaeozoic benthic faunas (and a sharp decrease in phosphorous contents, which are concentrated in skeletal fragments

of biota) occurs at the stratal interval 31–19 mm below the top of Bed 24e. After observing all samples from Bed 24 to Bed 29, we found that the disappearance boundary seen in the sample from the upper part of Bed 24e is the most distinct horizon where skeletal fragments of major fossil groups are abruptly eliminated. This distinct horizon is overlain by packstones enriched by Fe and Ni (Figs. 2, 3; Table 1). It is therefore unlikely that disappearance of calcareous fossil fragments at the top of layer 24e-2 was due to an increase in the input of terrestrial material associated with the facies shift. In addition, both layer 24e-2 and layer 24e-3 are bioclastic packstones. This means that sedimentary facies remained unchanged in both layers. Thus, facies change cannot explain adequately the abrupt disappearance of fossil fragments of major benthos. Alternatively, as discussed above, biotic mass extinction resulted in the reduction of skeleton contents in seawater. The sharp decline in abundance and diversity of fossil fragments between layer 24e-2 and layer 24e-3 likely signals the end-Permian mass extinction. Occurrence of abundant sponge spines above this event horizon was probably due to these tiny siliceous spines lasting in seawater for a while, although the sponge bodies died in the end-Permian extinction event. Accordingly, other than sponge spines, almost all benthos that proliferated previously in the pre-extinction ocean vanished immediately after the end-Permian event.

This event horizon is about 19 mm lower than the end-Permian mass extinction horizon calibrated by Jin et al. (2000) in the same section. In addition, the new extinction horizon is also coincident with the abrupt negative shift of $\delta^{34}S_{sulfate}$ values and anomalies of other elements (see below). If so, this extinction event occurred within a short period representing the sedimentation duration of the 12-mm-thick limestone layer, which is estimated to be deposited within <2 ky based on radiometric ages given above. Thus, this study supports the view that the end-Permian mass extinction is abrupt and catastrophic.

### 4.4. Sulfur isotope event

In Meishan, a remarkable decrease in $\delta^{34}S_{sulfate}$ in the ocean is revealed in layer 24e-2 (Kaiho et al., 2001) and, thus, coincides with the extinction horizon recognized under the microscope (Fig. 3; Table 1). This fact indicates that the end-Permian mass extinction is contemporaneous with the sulfur isotope event recognized from Meishan (Kaiho et al., 2001). These two contemporaneous events are also recognized from other P/Tr boundary sections around the world (i.e., Newton et al., 2004).

Where did the sulfur sources come from? Both an extraterrestrial impact to the oceanic crust and mantle plume-induced volcanic eruptions can release sulfur from the mantle. Recent studies reveal that either a comet impact upon the oceanic crust and mantle or the Siberian volcanic eruption can provide a huge amount of sulfur from the mantle to the atmosphere (Kaiho et al., 2001; Kamo et al., 2003). However, the Siberian flood basalt volcanism or a normal-sized comet (~10 km diameter) cannot supply enough sulfur to the atmosphere and ocean to cause a decrease in $\delta^{34}S_{sulfate}$ in the ocean. The amount of sulfur (over $10^{19}$ g of $SO_2$ (Kamo et al., 2003)) released from the Siberian volcanism is about 1/100 of sulfur in all sea water. Consequently, the release of sulfur from the mantle would not be a main cause of the decrease in $\delta^{34}S_{sulfate}$, although it may have accelerated the abrupt $\delta^{34}S_{sulfate}$ reduction.

Alternatively, such a huge amount of sulfur may have been sourced from an extraterrestrial impact to the oceanic crust. This inference is also evidenced by small but significant quantities of iridium (200 and 500 ppt) recorded in the P/Tr boundary beds in China (Clark et al., 1986) and Austria (Holser et al., 1989). Based on osmium isotope analyses, Koeberl et al. (2004) clarified that the PGE anomalies at the end of the Permian in Austria and Italy cannot be of meteorite or mantle origin. However, a decrease in $^{87}Sr/^{86}Sr$ ratio (Kaiho et al., 2001; Fig. 2) recorded in Bed 24e-3 of Meishan suggests injection of mantle material. Accordingly, additional osmium isotope analysis of other P/Tr boundary sections around the world is desirable to confirm Koeberl et al.'s clarification. In addition, the shocked quartz reported by Retallack et al. (1998) from the P/Tr boundary beds of Antarctica has been rejected by Langenhorst et al. (2005), and no real shocked quartz has been reported from the P/Tr sediments in other parts of the world. However, the absence of the shocked quartz may be due to an impact in oceanic crust and mantle which contains little quartz.

Like the Siberian flood basalt volcanism, a normal-sized comet (~10 km diameter) cannot supply enough sulfur to the atmosphere and ocean resulting in a decrease in $\delta^{34}S_{sulfate}$ in the ocean. The amount of sulfur released from the mantle melted by an impact of a normal-sized comet is also about 1/100 of sulfur in the entire sea waters. An impact of a maximum-sized comet (~20 km diameter) can supply only 1/10 of sulfur in the entire oceans. However, an impact of a large asteroid (>70 km diameter) can supply enough sulfur to cause the negative shift of $\delta^{34}S_{sulfate}$. As a result, we infer that an impact of a large asteroid (>70 km diameter) to the ocean crust may be responsible for the negative shift event of $\delta^{34}S_{sulfate}$,

although additional significant evidence is required from the P/Tr boundary beds worldwide to confirm this.

The negative shift of $\delta^{34}S$ sulfate was caused by an overturn of a stratified ocean dominated by $H_2S$ (Newton et al., 2004), implying coincidence of the mixed ocean and mass extinction. A presumed impact to the ocean can cause both ocean mixing and the mass extinction. Alternatively, Siberian flood basalt volcanism or related gas explosion (Morgan et al., 2004) may have triggered a long-term ($>10^3$ years) cooling leading to ocean mixing.

### 4.5. Origin of the gypsum

The value of $\delta^{34}S$ recorded for the overlying gypsum layer (25-2) is −15.8‰ vs. CDT. This gypsum layer is an oxidation product of oceanic sulfide (normally 20–60‰ lighter than oceanic sulfate), but was not directly originated from the mantle sulfide, which usually possesses a $\delta^{34}S$ ~0‰. Kaiho et al. (2002) interpreted the positive shift by 5–10‰ from ~20‰ to ~25–30‰ of the sulfate sulfur isotope ratio starting at 7 cm below the event layer (25-1) at Meishan as the result of sulfate reduction in a largely anoxic stratified ocean. Such a positive shift of sulfur isotope values also occurred just before the end-Permian mass extinction at Balvany, Hungary (23‰) and at the topmost Bellerophon Formation at Siusi, Italy (21‰; Newton et al., 2004). This fact indicates that oceanic anoxia predated slightly the end-Permian mass extinction worldwide (Erwin et al., 2002). The escalating accumulation of sulfide caused by the oceanic anoxia is a result of the enrichment of sulfate in the ocean, suggesting sulfur injection from the mantle (Kaiho et al., 2001; Maruoka et al., 2003). Liang (2002) demonstrated that strong acid rain and marine acidification occurred by hydrated sulfuric acid at the end of the Permian based on mineralogical evidence from Bed 25 in the Meishan section. Acid rain caused by a bolide impact or a volcanic eruption may have led to the accumulation of gypsum changed from the sulfide in the temporal oxic acidic ocean.

## 5. Conclusions

The end-Permian mass extinction horizon is calibrated, under a microscope, to a 12-mm stratal interval, 31–19 mm below the top of Bed 24e of the Changhsing Formation in the Meishan section. This extinction event is characterized by the abrupt disappearance of skeletal fragments of major benthos and was abrupt and catastrophic. The extinction horizon coincides with an abrupt decrease in the $^{34}S/^{32}S$ ratios of seawater sulfate, $^{87}Sr/^{86}Sr$ ratio, and an increase in Fe–Ni grains. These coincidences suggest that Siberian food basalt volcanism and related gas explosion and/or a comet impact to the ocean caused biotic mass extinction in the end of the Permian.

## Acknowledgements

We thank K. Tsukamoto for discussion, P. Gorjan, B. S. Cramer and two anonymous referees for comments on the manuscript. This work was supported by a Grant-in-Aid for scientific research from the Japan Society for the Promotion of Science (to KK and ZQC) and a discovery project from the Australian Research Council (to ZQC).

## References

Becker, L., Poreda, R.J., Hunt, A.G., Bunch, T.E., Rampino, M., 2001. Impact event at the Permian–Triassic boundary: evidence from extraterrestrial noble gases in fullerenes. Science 291, 1530–1533.

Becker, L., Poreda, R.J., Basu, A.R., Pope, K.O., Harrison, T.M., Nicholson, C., Iasky, R., 2004. Bedout: a possible end-Permian impact crater offshore of Northwestern Australia. Science 304, 1469–1476.

Bowring, S.A., Erwin, D.H., Jin, Y.G., Martin, M.W., David, E.K., Wang, W., 1998. U/Pb zircon geochronology and tempo of the end-Permian mass extinction. Science 280, 1039–1045.

Claoue-Long, J.C., Zhang, Z.C., Ma, G.G., Du, S.H., 1991. The age of the Permian–Triassic boundary. Earth Planet. Sci. Lett. 105, 182–190.

Clark, D.L., Wang, C.-Y., Orth, C.J., Gilmore, J.S., 1986. Conodont survival and low iridium abundances across the Permian–Triassic boundary in South China. Science 233, 984–986.

Erwin, D.H., 1993. The Great Paleozoic Crisis. Columbia University Press, New York. 327 pp.

Erwin, D.H., 1994. The Permo-Triassic extinction. Nature 367, 231–236.

Erwin, D.H., Bowring, S.A., Yugan, J., 2002. End-Permian mass extinctions: a review. In: Koeberl, MacLeod (Eds.), Catastrophic Events and Mass Extinctions: Impacts and Beyond Geological Society of America Special Paper, vol. 356, pp. 363–383.

Eshet, Y., Rampino, M.R., Visscher, H., 1995. Fungal event and palynological record of ecological crisis and recovery across the Permian–Triassic boundary. Geology 23, 967–970.

Grard, A., Francois, L.M., Dessert, C., Dupre, B., Godderis, Y., 2005. Basaltic volcanism and mass extinction at the Permo-Triassic boundary: environmental impact and modeling of the global carbon cycle. Earth Planet. Sci. Lett. 234, 207–221.

Grice, K., Cao, C., Love, G.D., Bottcher, M.E., Twitchett, R.J., Grosjean, E., Summons, R.E., Turgeon, S.C., Dunning, W., Jin, Y., 2005. Photic zone euxinia during the Permian–Triassic super-anoxic event. Science 307, 706–709.

Holser, W.T., Schönlaub, H.-P., Attrep, M., Boeckelmann, K., Klein, P., Magaritz, M., Orth, C.J., Fenninger, A., Jenny, C., Kralik, M., 1989. A unique geochemical record at the Permian/Triassic boundary. Nature 337, 39–44.

Huey, R.B., Ward, P.D., 2005. Hypoxia, global warming, and terrestrial Late Permian extinctions. Science 308, 398–401.

Ivanov, B.A., Melosh, H.J., 2003. Impacts do not initiate volcanic eruptions: eruptions close to the crater. Geology 31, 869–872.

Jin, Y.G., Wang, Y., Wang, W., Shang, Q.H., Cao, C.Q., Erwin, D.H., 2000. Pattern of marine mass extinction near the Permian–Triassic boundary in south China. Science 289, 432–436.

Kaiho, K., Kajiwara, Y., Nakano, T., Miura, Y., Kawahata, H., Tazaki, K., Ueshima, M., Chen, Z.Q., Shi, G.R., 2001. End-Permian catastrophe by a bolide impact: evidence of a gigantic release of sulfur from the mantle. Geology 29, 815–818.

Kaiho, K., Kajiwara, Y., Miura, Y., 2002. End-Permian catastrophe by a bolide impact: evidence of a gigantic release of sulfur from the mantle: comment and reply. Geology 30, 856.

Kamo, S.L., Czamanske, G.K., Amelin, Y., Fedorenko, V.A., Davis, D.W., Trofimov, V.R., 2003. Rapid eruption of Siberian flood-volcanic rocks and evidence for coincidence with the Permian–Triassic boundary and mass extinction at 251 Ma. Earth Planet. Sci. Lett. 214, 75–91.

Kidder, D.L., Worsley, T.R., 2004. Causes and consequences of extreme Permo-Triassic warming to globally equable climate and relation to the Permo-Triassic extinction and recovery. Palaeogeogr. Palaeoclimatol. Palaeoecol. 203, 207–237.

Knoll, A.K., Bambach, R.K., Canfield, D.E., Grotzinger, J.P., 1996. Comparative earth history and Late Permian mass extinction. Science 273, 452–457.

Koeberl, C., Gilmour, I., Reinold, W.U., Claeys, P., Ivanov, B., 2002. End-Permian catastrophe by a bolide impact: evidence of a gigantic release of sulfur from the mantle: comment and reply. Geology 30, 855–856.

Koeberl, C., Farley, K.A., Peucker-Ehrenbrink, B., Sephton, M.A., 2004. Geochemistry of the end-Permian extinction event in Austria and Italy: no evidence for an extraterrestrial component. Geology 32, 1053–1056.

Korte, C., Kozur, H.W., Joachimski, M.M., Strauss, H., Veizer, J., Schwark, L., 2004. Carbon, sulfur, oxygen and strontium isotope records, organic geochemistry and biostratigraphy across the Permian/Triassic boundary in Abadeh, Iran. Int. J. Earth Sci. 93, 565–581.

Langenhorst, F., Kyte, F.T., Retallack, G.L., 2005. Reexamination of quartz grains from the Permian–Triassic boundary section at Graphite peak, Antarctica. Lunar Planet. Sci. 36 (abs. No. 2358).

Liang, H., 2002. End-Permian catastrophic event of marine acidification by hydrated sulfuric acid: mineralogical evidence from Meishan section of South China. Chin. Sci. Bull. 47, 1393–1397.

Maruoka, T., Koeberl, C., Hancox, P.J., Reimold, W.U., et al., 2003. Sulfur geochemistry across a terrestrial Permian–Triassic boundary section in the Karoo Basin, South Africa. Earth Planet. Sci. Lett. 206, 101–117.

Morgan, J.P., Reston, T.J., Ranero, C.R., 2004. Contemporaneous mass extinctions, continental flood basalts, and cimpact signals□: are mantle plume-induced lithospheric gas explosions the causal link? Earth Planet. Sci. Lett. 217, 263–284.

Mundil, R., Metcalfe, I., Ludwig, K.R., Renne, P.R., Oberli, F., Nicoll, R.S., 2001. Timing of the Permian–Triassic biotic crisis: implications from new zircon U/Pb age data (and their limitations). Earth Planet. Sci. Lett. 187, 131–145.

Mundil, R., Ludwig, K.R., Metcalfe, I., Renne, P.R., 2004. Age and timing of the Permian mass extinctions. U/Pb dating of closed-system zircons. Science 305, 1760–1763.

Newton, R.J., Pevitt, E.L., Wignall, P.B., Bottrell, S.H., 2004. Large shifts in the isotopic composition of seawater sulphate across the Permo-Triassic boundary in northern Italy. Earth Planet. Sci. Lett. 218, 331–345.

Rampino, M.R., Adler, A.C., 1998. Evidence for abrupt latest Permian mass extinction of foraminifera: results of tests for the Signor–Lipps effect. Geology 26, 415–418.

Renne, P.R., Zichao, Z., Richards, M.A., Black, M.T., Basu, A.R., 1995. Synchrony and causal relations between Permian–Triassic boundary crisis and Siberian flood volcanism. Science 269, 1413–1416.

Retallack, G.J., 1995. Permian–Triassic extinction on land. Science 267, 77–80.

Retallack, G.J., Seyedolali, A., Krull, E.S., Holser, W.T., Ambers, C.P., Kyte, F.T., 1998. Search for evidence of impact at the Permian–Triassic boundary in Antarctica and Australia. Geology 26, 979–982.

Robinson, B.W., Kusakabe, M., 1975. Quantitative preparation of sulfur dioxide, for $^{34}S/^{32}S$ analyses, from sulfides by combustion with cuprous oxide. Anal. Chem. 47, 1179–1181.

Sasaki, A., Arikawa, Y., Folinsbee, R.E., 1979. Kiba reagent method of sulfur extraction applied to isotopic work. Bull. Geol. Surv. Jpn. 30, 241–245.

Wignall, P.B., 2001. Large igneous provinces and mass extinctions. Earth Sci. Rev. 53, 1–33.

Wignall, P.B., Twitchett, R.J., 1996. Oceanic anoxia and the end-Permian mass extinction. Science 272, 1155–1158.

Xie, S.C., Pancost, R.D., Yin, H.F., Wang, H.M., Evershed, R.P., 2005. Two episodes of microbial change coupled with Permo/Triassic faunal mass extinction. Nature 434, 494–497.

Yin, H.F., Wu, S.B., Ding, M.H., Zhang, K.X., Tong, J.N., Yang, F.Q., Lai, X.L., 1996. The Meishan section, candidate of the Global Stratotype Section and Point of Permian-Triassic Boundary. In: Yin, H.F. (Ed.), The Palaeozoic–Mesozoic Boundary Candidates of Global Stratotype Section and Point of the Permian–Triassic Boundary. NSFC Project. China University of Geosciences Press, Wuhan, China, pp. 31–48.

Yin, H.F., Zhang, K.X., Tong, J.N., Yang, Z.Y., Wu, S.B., 2001. The Global Stratotype Section and Point (GSSP) of the Permian–Triassic boundary. Episodes 24, 102–114.